IEEE Access
Multidisciplinary | Rapid Review | Open Access Journal

Received April 11, 2018, accepted May 20, 2018, date of publication May 25, 2018, date of current version June 19, 2018.

Digital Object Identifier 10.1109/ACCESS.2018.2840537

Concurrent Optimization for Selection and Control of AC Servomotors on the Powertrain of Industrial Robots

ERICK A. PADILLA-GARCIA[1], ALEJANDRO RODRIGUEZ-ANGELES[1], JUVENAL R. RESÉNDIZ[2], (Senior Member, IEEE), AND CARLOS A. CRUZ-VILLAR[1]

[1]Electrical Engineering Department, Mechatronics Section, CINVESTAV-IPN, Mexico 07360, Mexico
[2]Faculty of Engineering, Autonomous University of Queretaro, Querétaro 76010, Mexico

Corresponding author: Erick A. Padilla-Garcia (epadilla@cinvestav.mx)

This work was supported in part by the Program for the Professional Development Teacher, PRODEP, and in part by the National Council for Science and Technology, CONACyT, under Grant 254329.

ABSTRACT AC servomotors are widely used in industrial robot manipulators to drive high dynamic loads; thus, an appropriate selection and control of the motors contributes to a better performance at specific tasks. In this paper, a concurrent multi-objective dynamic optimization method is proposed for optimal selection and control of synchronous ac servomotors. Three objective functions, energy consumption, tracking error, and total weight of motors, are optimized. Regarding the importance of the reducers to drive the manipulator, our methodology considers as an equality constraint the closed-loop dynamic model of the whole system, where the powertrain (motor–reducer–load) at each actuated-joint is considered. The multi-objective optimization problem is solved by using a genetic algorithm with continuous and discrete variables. The efficiency of the proposed methodology is validated via simulations of an industrial robot.

INDEX TERMS Concurrent optimization, mechatronic design, ac servomotor selection, industrial manipulators, powertrain of robots.

I. INTRODUCTION

Industrial robots are used for many applications, such as handling, painting, assembling, welding and so on, where the efficiency and performance of the manipulator mainly depend on the dynamical response of its own drive system [1]. The needed drive energy is usually requested by the powertrain of the robot, which is composed of three subsystems at each actuated joint, servomotor, reducer, and load (Fig. 1).

Since the drive system has high impact in the dynamic response of the manipulator, the performance of an industrial robot can be improved by design and control optimization on the powertrain, being the motors the main sources of motion.

Traditionally, a design problem is solved independently of the control effects, thus leading to a non-optimal behavior [2]. However, a concurrent approach method deals with multi-objective optimization for simultaneous design and control, whose integration provides practical solutions to complex problems [3]. A common alternative solution for multi-objective optimization is by using evolutionary algorithms [4], [5], where a set of feasible solutions form the Pareto Front, letting the designer to select one of them to satisfy the proposed objectives subjectively.

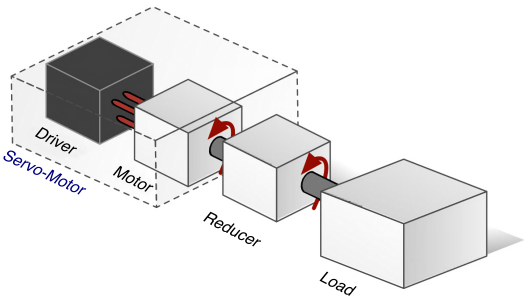

FIGURE 1. Powertrain on an actuated-joint.

In the same way, concurrent design optimization based on simulation model has become significant manufacturers methodology for the marketing of industrial robot products [6]. This because the trade-offs between objectives such as cost, performance, weight, energy, cost, accuracy, and so on, are essential for decisions that can be preceded by analyzing simulation models response. Thereby modeling, optimization, servo-design, model-based control, and identification have meant a breakthrough in industry, for proper

use of robots [7]. Moreover, new materials and technological advances keep open an essential challenge for industrial robotics, the optimal motor selection and control for a given application.

Most of motor selection methods use torque-level models, independently of the control inputs and regardless the electrical dynamics of the drive system (traditional design optimization), where candidate motors are determined by given static loads references or supposing that the working cycle to be performed by the powertrain is previously known. In [8] a motor torque is optimized for single axis case with a constant inertial load. Reference [9] obtains optimal motor/gear-ratio combination to drive a specific load, where the load cycle worst case is a priori known. Reference [10] proposed an optimal motor selection method for a given trajectory. In [11] a candidate motor can be selected from a graphical method, by separating the motor-load characteristics to get a parametrized curve for a given load. In [12] a torque-level motor selection is proposed for industrial manipulators, under the assumption that torque and motion cycles are independently known at each joint. In [6] design discrete variables are used to minimize the robot cost by selecting the lowest cost gearboxes for two axes of a manipulator. Similarly, in [13] discrete variables are also used to minimize the drive-train weight, where ADAMS simulator is used to know each required joint torque. Moreover, an extension of [11] is presented in [14], where new limits are added for both DC and AC servomotors, but interactions among actuators (such as those in a robotic arm) cannot be simultaneously considered for that methodology. In [15] design discrete variables are used to select motors and optimize working efficiency and natural frequency for a 4-DOF robot, by dynamic mechanical performance simulation.

Regarding motor types, it is preferred to operate AC servomotors instead of DC motors to drive high dynamic loads, due to higher torque-to-inertia ratio, higher peak torque capability and higher torque-speed bandwidth [11], [16], [17]. The most common kinds of AC servomotors for industrial applications are Induction Motors, three-phase Brushless DC Motors (BLDC), Switch Reluctance Motors, and Permanent Magnet Synchronous Motor (PMSM) [16]. From those, the PMSM motor type is proposed in this paper for a servomotor selection, since it has been widely employed for direct-drive industrial robots to provide high load, speed and accuracy requirements [18].

Because of the electrical complexity of AC servomotors, and considering that require control techniques unlike from those common applied for DC motors, few works have addressed robot dynamics with PMSM servomotors as a mechatronic system as in [18]. Nevertheless, high-performance designs are based on accurate knowledge of the dynamics of the system [19], so considering a mechatronic system has the advantage to analyze the dynamics response involved in the closed-loop drive system when different actuators are installed on the powertrain, ensuring that desired objectives for the task are being satisfied.

Our proposal integrates the optimal *off the shelf PMSM servomotor selection and control* in a single step, to provide to an existing robotic mechanism optimal performance for a particular task, by minimizing three objective functions, energy consumption, tracking error and total weight of motors, subject to the closed-loop mechatronic model of the robot, thus including the dynamic load profiles and control effects of the mechanism. This situation is, in fact, a significant advantage in manufacturing processes due to the repetitive nature of the robot performed tasks.

For the closed-loop dynamics, the control technique used for the selected AC servomotors is the Field Oriented Control technique (FOC), which is one of the most widely used in the industrial field since it maximizes torque efficiency and presents robustness to model parameters variations. Moreover, the FOC method does not require very sophisticated current sensors for control feedback and may ensure asymptotically tracking for the desired task [20], [21].

To avoid overexertion, heating or damage to the robotic system, thermal conditions, for continuous and instantaneous operating ranges of motors, are considered in our approach as constraints, based on [22]–[24] and [25], where these thermal conditions are dissected.

The proposed method is tested for an industrial robot manipulator real case. Here, the Non-dominated Sorting Genetic Algorithm (NSGA-II algorithm [26]) is used to solve the constrained multi-objective problem, which is an evolutionary algorithm extensively used to deal with concurrent multi-objective optimization problems [27]. Unlike other evolutionary algorithms, it provides solutions for the widespread distribution of the Pareto-front [28].

The rest of the article is organized as follows. In Section II, the mechatronic model of the case study is presented. Section III proposes the selection criteria for robot AC servomotors. Section IV shows the concurrent optimization approach. In Section V an application to a particular case is presented. Finally, in Section VI the article closes with some conclusions.

II. MECHATRONIC MODEL OF THE ROBOTIC SYSTEM

The mechatronic model-based design provides interaction across different sub-systems such as the mechanical, electrical and control dynamics of the robot to obtain concurrent solutions for the closed-loop system dynamics. This Section presents the different robot sub-systems involved in the proposed method.

A. DYNAMIC MODEL OF THE MANIPULATOR

Consider a rigid-link robot manipulator with n joints. The robot mechanism dynamics is given by

$$\boldsymbol{\tau} = \mathbf{M}(\mathbf{q})\,\ddot{\mathbf{q}} + \mathbf{C}(\mathbf{q}, \dot{\mathbf{q}})\dot{\mathbf{q}} + \mathbf{g}(\mathbf{q}), \tag{1}$$

where $\mathbf{q} \in \mathbb{R}^n$ is the generalized coordinates vector for all the mechanism joints, $\mathbf{M}(\mathbf{q}) \in \mathbb{R}^{n\times n}$ is the inertia matrix, $\mathbf{C}(\mathbf{q}, \dot{\mathbf{q}}) \in \mathbb{R}^{n\times n}$ is the Coriolis and centrifugal forces,

$\mathbf{g}(\mathbf{q}) \in \mathbb{R}^n$ the gravity terms vector and $\boldsymbol{\tau}(t) \in \mathbb{R}^n$ the input torques vector.

B. DYNAMIC MODEL OF THE POWERTRAIN

Let us suppose that from the robot manipulator with n joints, $\mathbf{q_a} \in \mathbb{R}^{n_a}$ are the actuated joints of the mechanism and $\mathbf{q_u} \in \mathbb{R}^{n-n_a}$ are the unactuated joints, i.e. $\mathbf{q} = [\mathbf{q_a}, \mathbf{q_u}] \in \mathbb{R}^n$. To generate the robot motion, the needed drive energy is requested by the powertrain of each actuated joint, which involves three parts, motor, reducer, and load (mechanism), as shown in Fig. 2.

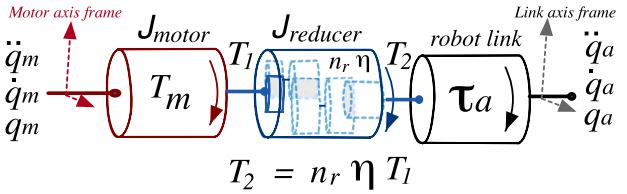

FIGURE 2. Schematic view of the powertrain model for an actuated joint.

The k-th actuated joint of the powertrain requires a motor torque $T_{m,k}(t)$ to drive the load profile $\tau_{a,k}(t)$, as

$$T_{m,k} = J_{eq,k} n_{r,k} \ddot{q}_{a,k} + b_{eq,k} n_{r,k} \dot{q}_{a,k} + \frac{\tau_{a,k}}{n_{r,k}\eta_k}, \tag{2}$$

where η_k is the transmission torque efficiency in the reducer, $n_{r,k}$ is the reducer's transmission ratio, $J_{eq,k}$ and $b_{eq,k}$ are the equivalent inertia and viscous friction obtained as

$$J_{eq,k} = J_{motor,k} + J_{reducer,k}, \tag{3}$$
$$b_{eq,k} = b_{motor,k} + b_{reducer,k}, \tag{4}$$

for $k = 1, \ldots, n_a$.

Moreover, assume that motor-reducer position relationships fulfill that

$$q_{m,k} = n_{r,k} q_{a,k}, \tag{5}$$

where $q_{m,k}$ is the k-th angular rotor position, viewed at the motor axis, and $q_{a,k}$ the angular position of each actuated joint, viewed at the robot link axis.

Then, the powertrain dynamics is given by

$$\mathbf{T_m} = \mathbf{J}_{eq}\boldsymbol{\Phi}\ddot{\mathbf{q}}_\mathbf{a} + \mathbf{B}_{eq}\boldsymbol{\Phi}\dot{\mathbf{q}}_\mathbf{a} + [\boldsymbol{\Phi}\boldsymbol{\Upsilon}]^{-1}\boldsymbol{\tau}_\mathbf{a}, \tag{6}$$

where $\boldsymbol{\Phi} = \text{diag}\{[n_{r,1}, \ldots, n_{r,n_a}]\}$, $\boldsymbol{\Upsilon} = \text{diag}\{[\eta_1, \ldots, \eta_{n_a}]\}$, $\mathbf{T_m} = [T_{m,1}, \ldots, T_{m,n_a}]^T$, $\mathbf{J}_{eq} = \text{diag}\{[J_{eq,1}, \ldots, J_{eq,n_a}]\}$, $\mathbf{B}_{eq} = \text{diag}\{[b_{eq,1}, \ldots, b_{eq,n_a}]\}$. $\boldsymbol{\tau}_\mathbf{a} = [\tau_{a,1}, \ldots, \tau_{a,n_a}]^T$ is the load torques vector of the actuated joints. For simplicity, the time dependence notation is omitted.

C. DYNAMIC MODEL OF THE ROBOT CONSIDERING THE POWERTRAIN DYNAMICS

Independently of the kind of kinematic chain (serial or parallel) and according to [29]–[31], a functional relationship, between all the joint variables (actuated and unactuated), can be obtained in terms of the actuated joints as $q_i = \mathcal{Q}_i(\mathbf{q_a})$. Thus, the joint variables of the mechanism can be expressed by

$$\mathbf{q} = \mathcal{Q}(\mathbf{q_a}). \tag{7}$$

The velocities and accelerations in terms of the actuated joints can be obtained as

$$\dot{\mathbf{q}} = \boldsymbol{\Psi}\dot{\mathbf{q}}_\mathbf{a}, \tag{8}$$
$$\ddot{\mathbf{q}} = \dot{\boldsymbol{\Psi}}\dot{\mathbf{q}}_\mathbf{a} + \boldsymbol{\Psi}\ddot{\mathbf{q}}_\mathbf{a}, \tag{9}$$

where

$$\boldsymbol{\Psi}_{ij} = \frac{\partial \mathcal{Q}_i(\mathbf{q_a})}{\partial \mathbf{q_a}_j}, \quad i = 1, \ldots, n,\ j = 1, \ldots, n_a. \tag{10}$$

$\boldsymbol{\Psi} \in \mathbb{R}^{n \times n_a}$ is the transformation matrix relating all the robot joints in terms of the actuated joints. By using the kineto-statics duality concept [29], it is possible to establish the relationship

$$\boldsymbol{\tau}_\mathbf{a} = \boldsymbol{\Psi}^T\boldsymbol{\tau}, \tag{11}$$

where $\boldsymbol{\tau}_\mathbf{a} \in \mathbb{R}^{n_a}$ is the torques vector of the actuated joints from $\boldsymbol{\tau} \in \mathbb{R}^n$. Thus, the torques vector of the unactuated joints is $\boldsymbol{\tau}_\mathbf{u} = [0, 0, \ldots, 0] \in \mathbb{R}^{n-n_a}$.

From above, the dynamic model of the manipulator can be expressed in terms of the actuated joints, by using (7), (8) and (9) in (1), and substituting it in (11), then

$$\boldsymbol{\tau}_\mathbf{a} = \mathbf{M_A}(\mathbf{q_a})\,\ddot{\mathbf{q}}_\mathbf{a} + \mathbf{C_A}(\mathbf{q_a}, \dot{\mathbf{q}}_\mathbf{a})\dot{\mathbf{q}}_\mathbf{a} + \mathbf{g_A}(\mathbf{q_a}), \tag{12}$$

where

$$\mathbf{M_A}(\mathbf{q_a}) = \boldsymbol{\Psi}^T\mathbf{M}(\mathcal{Q}(\mathbf{q_a}))\,\boldsymbol{\Psi}, \tag{13}$$
$$\mathbf{C_A}(\mathbf{q_a}, \dot{\mathbf{q}}_\mathbf{a}) = \mathbf{C_0} + \boldsymbol{\Psi}^T\mathbf{C}(\mathcal{Q}(\mathbf{q_a}), \boldsymbol{\Psi}\dot{\mathbf{q}}_\mathbf{a})\boldsymbol{\Psi}, \tag{14}$$
$$\mathbf{g_A}(\mathbf{q_a}) = \boldsymbol{\Psi}^T\mathbf{g}(\mathcal{Q}(\mathbf{q_a})), \tag{15}$$

and

$$\mathbf{C_0} = \boldsymbol{\Psi}^T\mathbf{M}(\mathcal{Q}(\mathbf{q_a}))\,\dot{\boldsymbol{\Psi}}, \tag{16}$$

where $\mathbf{M_A} \in \mathbb{R}^{n_a \times n_a}$, $\mathbf{C_A} \in \mathbb{R}^{n_a \times n_a}$ and $\mathbf{g_A} \in \mathbb{R}^{n_a \times 1}$. Typically, due to the industrial anthropomorphic arms structure, $\boldsymbol{\Psi}$ results a constant matrix, which means that $\mathbf{C_0} = \mathbf{0}$.

Now, the mechanism dynamics $\boldsymbol{\tau}_\mathbf{a}$, obtained in (12), can be directly related to the powertrain dynamics $\mathbf{T_m}$, given by (6), as

$$\mathbf{T_m} = \mathbf{H}(\mathbf{q_a})\,\ddot{\mathbf{q}}_\mathbf{a} + \mathbf{D}(\mathbf{q_a}, \dot{\mathbf{q}}_\mathbf{a})\dot{\mathbf{q}}_\mathbf{a} + \mathbf{F_R}\dot{\mathbf{q}}_\mathbf{a} + \mathbf{G}(\mathbf{q_a}), \tag{17}$$

where

$$\mathbf{H}(\mathbf{q_a}) = \left[\mathbf{J}_{eq}\boldsymbol{\Phi} + (\boldsymbol{\Phi}\boldsymbol{\Upsilon})^{-1}\mathbf{M_A}(\mathbf{q_a})\right], \tag{18}$$
$$\mathbf{D}(\mathbf{q_a}, \dot{\mathbf{q}}_\mathbf{a}) = \left[(\boldsymbol{\Phi}\boldsymbol{\Upsilon})^{-1}\mathbf{C_A}(\mathbf{q_a}, \dot{\mathbf{q}}_\mathbf{a})\right], \tag{19}$$
$$\mathbf{F_R} = \left[\mathbf{B}_{eq}\boldsymbol{\Phi}\right], \tag{20}$$
$$\mathbf{G}(\mathbf{q_a}) = \left[(\boldsymbol{\Phi}\boldsymbol{\Upsilon})^{-1}\mathbf{g_A}(\mathbf{q_a})\right]. \tag{21}$$

D. ELECTRICAL DYNAMIC MODEL OF ACTUATORS

Let us consider that the actuators in the powertrain are motors of type PMSM, under the following considerations,

- Motor windings are symmetrically designed and distributed.
- The magnetic circuit is unsaturated.
- Changes in electrical parameter values, such as eddy current and hysteresis losses are negligible.
- Three-phase stator windings are sinusoidally distributed.
- The relationship between the winding position θ_e and the angular rotor position q_m, is $\theta_e = n_P q_m$, where n_P is the number of motor pair poles.

Considering the motor-reducer position relationship in (5), the k-th electrical winding position $\theta_{e,k}$ can be written in terms of the k-th actuated joint $q_{a,k}$, as

$$\theta_{e,k} = n_{P,k} q_{m,k} = n_{P,k} n_{r,k} q_{a,k} \text{ for } k = 1, \ldots, n_a. \quad (22)$$

By using the Clarke and Park Transformations [16], as

$$T_p = \frac{2}{3}\begin{bmatrix} \cos(\theta_{e,k}) & \cos(\theta_{e,k} - \frac{2}{3}\pi) & \cos(\theta_{e,k} + \frac{2}{3}\pi) \\ sin(\theta_{e,k}) & sin(\theta_{e,k} - \frac{2}{3}\pi) & sin(\theta_{e,k} + \frac{2}{3}\pi) \\ \frac{1}{2} & \frac{1}{2} & \frac{1}{2} \end{bmatrix} \quad (23)$$

the three-phase frame electrical equations of each motor can be represented in a two-phase orthogonal frame (q, d) with a balanced homopolar phase, where the current vector in the (q, d) frame is static, and voltages can be operated as DC inputs, rather than sinusoidal signals [16].

From above, the electrical dynamic equations for each motor in the (q, d) frame from the three-phase frame are

$$v_{q,k} = R_{s,k} i_{q,k} + \frac{d}{dt}\lambda_{q,k} + n_{P,k} n_{r,k} \dot{q}_{a,k} \lambda_{d,k}, \quad (24)$$

$$v_{d,k} = R_{s,k} i_{d,k} + \frac{d}{dt}\lambda_{d,k} - n_{P,k} n_{r,k} \dot{q}_{a,k} \lambda_{q,k}, \quad (25)$$

and

$$\lambda_{q,k} = L_{q,k} i_{q,k}, \quad (26)$$

$$\lambda_{d,k} = L_{d,k} i_{d,k} + \lambda_{af,k}, \quad (27)$$

where for the k-th actuated-joint, $v_{q,k}$ and $v_{d,k}$ are the frame voltages, $i_{q,k}$ and $i_{d,k}$ are the frame currents of the motor, $L_{q,k}$ and $L_{d,k}$ are the frame inductances, $R_{s,k}$ is the resistance of stator windings, $\lambda_{af,k}$ the flux amplitude induced to the phases of the stator by the rotor magnets, and the electromechanical torque of each motor can be obtained as

$$T_{m,k} = \frac{3}{2} n_{P,k} n_{r,k} [\lambda_{af,k} + (L_{d,k} - L_{q,k}) i_{d,k}] i_{q,k}. \quad (28)$$

Due to the symmetrical and sinusoidal distribution of windings, the inductances $L_{q,k}$ and $L_{d,k}$ in the (q, d) frame can be considered constants [16]. Then, solving the electrical equations depending on the currents and reordering terms, the electrical dynamics for each motor can be

$$\frac{d}{dt} i_{q,k} = \frac{1}{L_{q,k}} [v_{q,k} - R_{s,k} i_{q,k} - n_{P,k} n_{r,k} \dot{q}_{a,k} L_{d,k} i_{d,k} - n_{P,k} n_{r,k} \dot{q}_{a,k} \lambda_{af,k}], \quad (29)$$

$$\frac{d}{dt} i_{d,k} = \frac{1}{L_{d,k}} [v_{d,k} - R_{s,k} i_{d,k} + n_{P,k} n_{r,k} \dot{q}_{a,k} L_{q,k} i_{q,k}], \quad (30)$$

$$T_{m,k} = \frac{3}{2} n_{P,k} n_{r,k} [\lambda_{af,k} + (L_{d,k} - L_{q,k}) i_{d,k}] i_{q,k}. \quad (31)$$

Then, the whole electrical dynamics, for all the motors on the powertrain, can be expressed as follows (this form has been used for direct-drive robots with PMSM motors, as in [18]),

$$\dot{\mathbf{I}}_\mathbf{q} = \mathbf{L}_\mathbf{q}^{-1} [\mathbf{V_q} - \mathbf{R_s} \mathbf{I_q} - \mathbf{\Theta \Phi L_d} \boldsymbol{\sigma} - \mathbf{\Theta \Phi \Lambda_{af}} \dot{\mathbf{q}}_\mathbf{a}] \quad (32)$$

$$\dot{\mathbf{I}}_\mathbf{d} = \mathbf{L}_\mathbf{d}^{-1} [\mathbf{V_d} - \mathbf{R_s} \mathbf{I_d} + \Theta \Phi \mathbf{L_q} \boldsymbol{\varrho}] \quad (33)$$

$$\mathbf{T_m} = \frac{3}{2} \mathbf{\Theta \Phi} [\mathbf{\Lambda_{af}} \mathbf{I_q} + \mathbf{L_d} \boldsymbol{\zeta} - \mathbf{L_q} \boldsymbol{\zeta}] \quad (34)$$

where $\mathbf{I_q} = [i_{q,1}, i_{q,2}, \ldots, i_{q,n_a}]^T$, $\mathbf{I_d} = [i_{d,1}, \ldots, i_{d,n_a}]^T$, $\mathbf{V_d} = [v_{d,1}, \ldots, v_{d,n_a}]^T$, $\mathbf{\Lambda_{af}} = \text{diag}\{[\lambda_{af,1}, \ldots, \lambda_{af,n_a}]\}$, $\mathbf{R_s} = \text{diag}\{[R_{s,1}, \ldots, R_{s,n_a}]\}$, $\mathbf{\Theta} = \text{diag}\{[n_{P,1}, \ldots, n_{P,n_a}]\}$, $\mathbf{L_d} = \text{diag}\{[L_{d,1}, \ldots, L_{d,n_a}]\}$, $\mathbf{V_q} = [v_{q,1}, v_{q,2} \ldots, v_{q,n_a}]^T$, and $\mathbf{L_q} = \text{diag}\{[L_{q,1}, \ldots, L_{q,n_a}]\}$. The vectors $\boldsymbol{\sigma} \in \mathbb{R}^{n_a}$, $\boldsymbol{\varrho} \in \mathbb{R}^{n_a}$, and $\boldsymbol{\zeta} \in \mathbb{R}^{n_a}$ are defined by the k-th element of the vector as

$$\sigma_k = i_{d,k} \dot{q}_{a,k}, \quad (35)$$

$$\varrho_k = i_{q,k} \dot{q}_{a,k}, \quad (36)$$

$$\zeta_k = i_{d,k} i_{q,k}. \quad (37)$$

In order to obtain the characteristics in the three-phase frame (a, b, c) from the (q, d) frame, and vice versa, let us suppose that S represents a vector of any of the physical characteristics such as motor currents, voltages, and flux of the magnetic fields of the motor; then, the transformation matrix in (23) can be used, where $S(q, d, 0) = T_p \cdot S(a, b, c)$ and $S(a, b, c) = T_p^{-1} \cdot S(q, d, 0)$.

E. CONTROL OF ACTUATORS IN THE POWERTRAIN

To consider the mechatronic system, in a closed-loop dynamics, the FOC control is used, since is one of the most widely used control methods in the industry for PMSM motors, and it has been intensely studied in the literature [16], [20]. Basically, FOC method consists of two internal current loops, by using two PI voltage controllers, and an external loop for torque-position control, see Fig. 3.

For each k-th motor, the (q, d) frame control voltages, $v_{q,k}^*$ and $v_{d,k}^*$, are proposed as PI controller; then, the voltage vectors $\mathbf{V_q^*}$ and $\mathbf{V_d^*}$, are proposed as follows (for more details of the FOC control method in [16]),

$$\mathbf{V_q^*} = \mathbf{K}_{p,q} (\mathbf{I_q^*} - \mathbf{I_q}) + \mathbf{K}_{I,q} \int_o^{t_f} (\mathbf{I_q^*} - \mathbf{I_q}) dt, \quad (38)$$

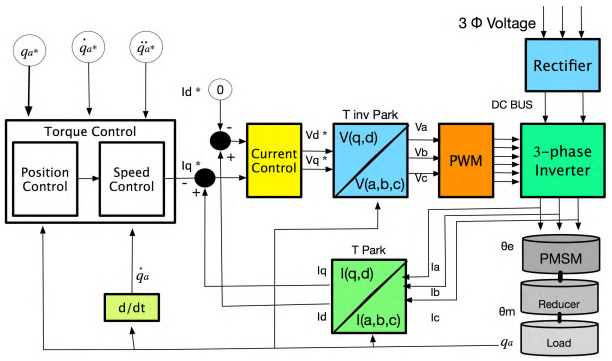

FIGURE 3. Field oriented control on an actuated joint.

$$\mathbf{V_d^*} = \mathbf{K}_{p,d}(\mathbf{I_d^*} - \mathbf{I_d}) + \mathbf{K}_{I,d}\int_o^{t_f}(\mathbf{I_d^*} - \mathbf{I_d})dt, \quad (39)$$

where $\mathbf{K}_{p,q}$, $\mathbf{K}_{p,d}$, $\mathbf{K}_{I,q}$, and $\mathbf{K}_{I,d}$ are positive definite diagonal matrices and t_f is the cycle time of the desired task. $\mathbf{I_q^*}$ and $\mathbf{I_d^*}$ are desired currents vectors given by

$$\mathbf{I_q^*} = \frac{2}{3}[\mathbf{\Theta\Phi\Lambda_{af}}]^{-1}\mathbf{T_m^*}, \quad (40)$$

$$\mathbf{I_d^*} = \mathbf{0}, \quad (41)$$

where $\mathbf{T_m^*}$ is the desired mechanical motor torques vector on the powertrain, to drive the given load of the mechanism. Since the currents in the (q, d) frame are static, the PI voltage controllers operate as DC inputs, instead of sinusoidal as in the three-phase frame. This transformation isolates the control signals from the time-variant winding, and as a result of that, the control method in the (q, d) frame eliminates the phase shift on motor.

Since the magnetic field is the direct result of current in the coils, if $\mathbf{I_d}$ tends to zero (i.e. $\mathbf{I_d^*}$), and $\mathbf{I_q}$ tends to $\mathbf{I_q^*}$, it is said that the current space vector is exclusively in the quadrature direction, and as a result of this, the torque efficiency is maximized, i.e. $\mathbf{T_m}$, given by (34), tends to the desired mechanical torque $\mathbf{T_m^*}$. This desired torque is proposed by the user and it can be designed as follows.

Suppose that $\ddot{\mathbf{q}}_\mathbf{a}^*$, $\dot{\mathbf{q}}_\mathbf{a}^*$, and $\mathbf{q_a^*}$ are the desired angular acceleration, velocity and position, respectively of the actuated joints. Then, the position and velocity errors are

$$\mathbf{e} = \mathbf{q_a^*} - \mathbf{q_a}, \quad (42)$$

$$\dot{\mathbf{e}} = \dot{\mathbf{q}}_\mathbf{a}^* - \dot{\mathbf{q}}_\mathbf{a}. \quad (43)$$

In order to cancel the non-linearities, the desired control torque $\mathbf{T_m^*}$ is designed as

$$\mathbf{T_m}^* = \mathbf{H}(\mathbf{q_a})(\ddot{\mathbf{q}}_\mathbf{a}^* + \mathbf{K_1 e} + \mathbf{K_2}\dot{\mathbf{e}}) + \mathbf{D}(\mathbf{q_a}, \dot{\mathbf{q}}_\mathbf{a})\dot{\mathbf{q}}_\mathbf{a} + \mathbf{F_R}\dot{\mathbf{q}}_\mathbf{a} + \mathbf{G}(\mathbf{q_a}), \quad (44)$$

substituting $\mathbf{T_m^*}$ in the mechanical dynamic model of the robot (17), the closed-loop system becomes

$$\ddot{\mathbf{e}} = -\mathbf{K_1 e} - \mathbf{K_2}\dot{\mathbf{e}}. \quad (45)$$

which is asymptotically stable for $\mathbf{K}_1$, $\mathbf{K}_2$ positive definite diagonal matrices. Therefore, the tracking errors tend to zero when time tends to infinity.

F. MECHATRONIC MODEL OF THE ROBOTIC SYSTEM

Considering the electrical and mechanical dynamics of the whole robot, and the field oriented control at each actuated joint, the closed-loop dynamic model can be written as

$$\ddot{\mathbf{q}}_\mathbf{a} = \mathbf{H}(\mathbf{q_a})^{-1}[\mathbf{T_m} - \mathbf{D}(\mathbf{q_a}, \dot{\mathbf{q}}_\mathbf{a})\dot{\mathbf{q}}_\mathbf{a} - \mathbf{F}\dot{\mathbf{q}}_\mathbf{a} - \mathbf{G}(\mathbf{q_a})] \quad (46)$$

$$\mathbf{T_m} = \frac{3}{2}\mathbf{\Theta\Phi}[\mathbf{\Lambda_{af}I_q} + \mathbf{L_d}\boldsymbol{\zeta} - \mathbf{L_q}\boldsymbol{\zeta}] \quad (47)$$

$$\dot{\mathbf{I}}_\mathbf{q} = \mathbf{L_q^{-1}}[\mathbf{V_q^*} - \mathbf{R_s I_q} - \mathbf{\Theta\Phi L_d}\boldsymbol{\sigma} - \mathbf{\Theta\Phi\Lambda_{af}}\dot{\mathbf{q}}_\mathbf{a}] \quad (48)$$

$$\dot{\mathbf{I}}_\mathbf{d} = \mathbf{L_d^{-1}}[\mathbf{V_d^*} - \mathbf{R_s I_d} + \mathbf{\Theta\Phi L_q}\boldsymbol{\varrho}] \quad (49)$$

where $\mathbf{V}_q^*$ and $\mathbf{V}_d^*$ are the control voltages of the FOC control required to do the desired task.

III. MOTOR SELECTION AND CONTROL CONSTRAINTS

The proposed methodology is based on selection and control of a proper set of off the shelf motors. Then, by using the mechatronic model of the robot, the different motor candidates can be evaluated and compared to get feasible solutions.

It is assumed that motor parameters and limit values for safe motor operation are available at manufacturers' catalogs; thus, selecting a motor parameterizes the powertrain, and the mechanical and electrical limits constrain the motor operation ranges.

A. PARAMETERS, LIMITS, AND RANGES OF FEASIBLE MOTORS

1) PARAMETERS

The required information from manufacturers' catalogs, to parameterize the proposed powertrain model, is the following.

- Mass m_m
- Rotor inertia J_{motor}
- Number of pair poles n_P
- Motor dimensions (motor size)
- Phase-to-phase inductance L_s
- Phase-to-phase resistance R_s
- The voltage constant that relates voltage-velocity V_E

The parameterization gives a specific model of the system, and as a consequence of that, a particular behavior is obtained for currents $\mathbf{I_q}$, $\mathbf{I_d}$, and torques $\mathbf{T_m}$ while driving the motors with $\mathbf{V_q^*}$, $\mathbf{V_d^*}$.

2) MECHANICAL AND ELECTRICAL LIMITS

Considering the control inputs, the required information from manufacturers' catalogs to safely drive the motors of the powertrain is

- Maximum torque $T_{M,max}$
- Continuous torque $T_{M,N}$
- Maximum velocity $\omega_{M,max}$
- Continuous velocity $\omega_{M,N}$

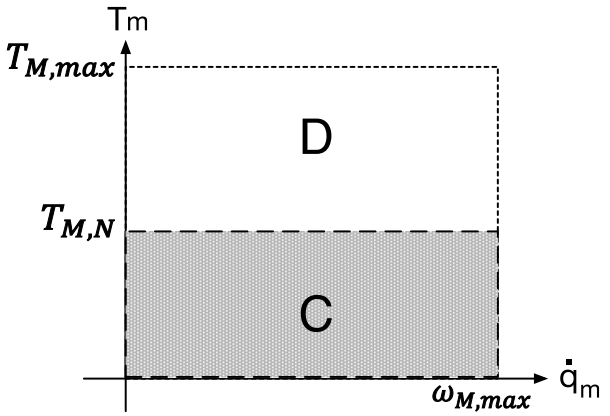

FIGURE 4. Continuous and dynamic operating zones in a $(\dot{q}_m, T_m)$-graph.

- Maximum current I_{max}
- Continuous current I_N
- Voltage bus to operate the motor V_{bus}
- Nominal power P_N
- Continuous voltage V_N

These limits are used as feasibility constraints to determine each candidate motor for the required task.

3) CONTINUOUS AND DYNAMIC RANGES OF FEASIBLE MOTORS

In a typical velocity-torque curve $(\dot{q}_m, T_m)$, two operating zones can be bounded, the *continuous operation zone* (C), limited by the continuous torque $T_{M,N}$, and the *dynamic operation zone* (D) which is limited by the maximum torque $T_{M,max}$ (Fig. 4).

In the continuous zone, the motor provides torque during long time without over-heating, covering the entire velocity range, limited by $\omega_{M,max}$. This fact, can be contrasted with the produced steady-state torque $T_{m,rms}$, which is produced by the same amount of heat during periods of continuous time and is given by

$$T_{m,rms} = \sqrt{\frac{1}{t_f}\int_0^{t_f} \{T_m\}^2 dt}, \tag{50}$$

where t_f is the cycle time of the task and T_m is the motor torque obtained by (17).

Similarly, the voltage and current at steady-state V_{rms} and I_{rms}, produce the same heat dissipation during the motor operation that can be equated with the limits $V_{N,M}$ and $I_{N,M}$ where

$$V_{rms} = \sqrt{\frac{1}{t_f}\int_0^{t_f} V_m^2 dt} = \sqrt{\frac{1}{t_f}\int_0^{t_f} \{v_q^2 + v_d^2\} dt}, \tag{51}$$

and

$$I_{rms} = \sqrt{\frac{1}{t_f}\int_0^{t_f} I_m^2 dt} = \sqrt{\frac{1}{t_f}\int_0^{t_f} \{i_q^2 + i_d^2\} dt}. \tag{52}$$

In the dynamic zone, the motor can momentarily operate at maximum torque and velocity values that can be obtained as

$$\|T_m\|_\infty = \max\{|T_m|\}, \tag{53}$$
$$\|\omega_m\|_\infty = \max\{|\dot{q}_a \cdot n_r|\}, \tag{54}$$

where the dynamic range to drive the motor for short periods of time can be contrasted with the torque and speed limits $T_{M,max}$ and $\omega_{M,max}$. Likewise, the electrical maximum voltage and current are obtained as

$$\|V_m\|_\infty = \max\{\left|\sqrt{v_q^2 + v_d^2}\right|\}, \tag{55}$$
$$\|I_m\|_\infty = \max\{\left|\sqrt{i_q^2 + i_d^2}\right|\}, \tag{56}$$

whose values can be equated with the limits of electrical dynamic operation range V_{max} and I_{max} .

B. FEASIBLE MOTOR CONSTRAINTS

Based on above characteristics, a feasibility criterion can be proposed and considered as a constraint to the selection and control process to avoid overheating and overexertion on the powertrain. Then, the requirements for a feasible candidate motor at each k-th actuated joint are the following (for simplicity, motor index k is omitted in this section).

1) MECHANICAL MOTOR CHARACTERISTICS

$$\text{Continuous torque: } T_{M,N} \geq \sqrt{\frac{1}{t_f}\int_0^{t_f} \{T_m\}^2 dt}, \tag{57}$$
$$\text{Maximum speed: } \omega_{M,max} \geq \max\{|\dot{q}_a \cdot n_r|\}, \tag{58}$$
$$\text{Maximum torque: } T_{M,max} \geq \max\{|T_m|\}, \tag{59}$$

where each motor torque T_m can be obtained from (17).

2) ELECTRICAL MOTOR CHARACTERISTICS

$$\text{Continuous current : } I_N \geq \sqrt{\frac{1}{t_f}\int_0^{t_f} \{i_q^2 + i_d^2\} dt}, \tag{60}$$
$$\text{Maximum current : } I_{max} \geq \max\{\left|\sqrt{i_q^2 + i_d^2}\right|\}, \tag{61}$$
$$\text{Continuous voltage : } V_N \geq \sqrt{\frac{1}{t_f}\int_0^{t_f} \{v_q^2 + v_d^2\} dt}, \tag{62}$$
$$\text{Maximum voltage : } V_{max} \geq \max\{\left|\sqrt{v_q^2 + v_d^2}\right|\}. \tag{63}$$

3) TRANSMISSION CHARACTERISTICS

$$\text{maximum load torque: } T_{G,max} \geq \max\{|\tau_a(t)|\}, \tag{64}$$
$$\text{maximum input speed: } \omega_{G,max} \geq \max\{|\dot{q}_a \cdot n_r|\}, \tag{65}$$

where each load torque can be given by (12). $T_{G,max}$ and $\omega_{G,max}$ are limit values for load torques and coupling speed on the powertrains' transmission or reducer.

C. PARAMETER CHANGES IN ROBOT DYNAMICS

The governing dynamic equation of the mechanism (1) can be obtained by using the Euler–Lagrange formulation [29]. In general, the inertia matrix, $\mathbf{M}(\mathbf{q})$, can be obtained by

$$\mathbf{M}(\mathbf{q}) = \sum_{i=1}^{n} \left(\mathbf{J}_{\mathbf{v}_{ci}}^{T} m_i \mathbf{J}_{\mathbf{v}_{ci}} + \mathbf{J}_{\boldsymbol{\omega}_i}^{T} \mathbf{I}_i \mathbf{J}_{\boldsymbol{\omega}_i} \right). \tag{66}$$

$\mathbf{J}_{\mathbf{v_{ci}}} \in \mathbb{R}^{3\times n}$ and $\mathbf{J}_{\omega,\mathbf{i}} \in \mathbb{R}^{3\times n}$ are the linear and angular Jacobian matrices related to the mass center $\mathbf{O}_{ci}$ of the i-th link of the robot, and $\mathbf{I}_i$ is the inertia tensor matrix for the i-th link related to the base frame, given by

$$\mathbf{I}_i = \mathbf{R}_i \mathbf{I}_i^i \mathbf{R}_i^T. \tag{67}$$

where $\mathbf{R}_i$ is the rotation matrix with respect the base frame and $\mathbf{I}_i^i$ is the inertia tensor with respect to the i-th center mass local frame.

The Coriolis matrix $\mathbf{C}(\mathbf{q}, \dot{\mathbf{q}})$ can be computed from the Inertia matrix values of (63) (for example, obtaining the first type Christoffel symbols [29]), and the i-th element of the gravity vector $\mathbf{g}(\mathbf{q})$, can be obtained as

$$g_i(\mathbf{q}) = \frac{\partial}{\partial q_i} \sum_{j=1}^{n} m_j \mathbf{g_0}^T \mathbf{O}_{cj}. \tag{68}$$

where $\mathbf{g_0}$ represents the gravity acceleration vector with respect the base of the robot ($\mathbf{g_0} = [0, 0, -g]^T$ if the gravity vector is acting on z axis).

Suppose that we are selecting motors on the powertrain for a fixed manipulator structure. Then, notice that (66), (67) and (68) depend on the inertial parameters values m_i, $\mathbf{O}_{ci}$, and $\mathbf{I}_i$ at each link of the manipulator. However, the total mass of each link m_i changes because of the installed motors on the mechanism, and it also modifies the mass center location $\mathbf{O}_{ci}$ concerning the local frame. Moreover, each added motor has an associated tensor of inertia, such that it affects to the total inertial $\mathbf{I}_i$ in the local link. Therefore, the dynamics equations of the manipulator are affected by the powertrain parameterization, where the inertial parameters values m_i, $\mathbf{O}_{ci}$ and $\mathbf{I}_i$ changes at each link of the manipulator. These effects are considered in this paper as follows.

1) MASS CHANGES

Since there are robot structures with more than one motor installed on the same link, the total mass of the i-th link changes (where $i = 1, \ldots, n$), that modification can be calculated as

$$m_i = \sum_{j=1}^{p} m_{i,j} \tag{69}$$

where $m_{i,j}$ is the mass contribution of the j-th element (link and added motors) to the i-th link of the robot.

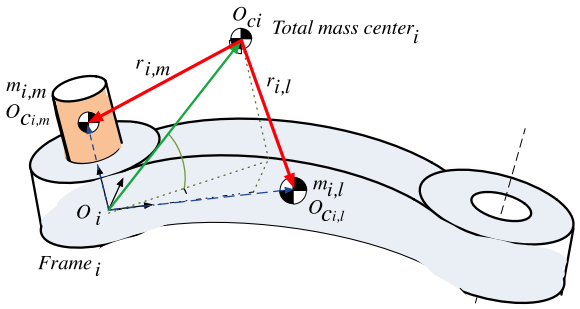

FIGURE 5. Mass center position of the j-th motor related to the i-th frame.

2) MASS CENTER LOCATION

For the i-th link of the robot, the mass center location, denoted by $\mathbf{O_{ci}}$, can be obtained as

$$\mathbf{O_{ci}} = \frac{1}{m_i} \sum_{j=1}^{p} \mathbf{O_{c_{i,j}}} m_{i,j} \tag{70}$$

where $\mathbf{O_{c_{i,j}}}$ is the mass location vector of the j-th element with respect to the i-th local frame.

3) TOTAL INERTIA

Considering that the inertia of each link modifies the dynamic model of the robot, it is necessary to consider these inertial changes, which can be obtained by using the *Steiner's theorem* as follows.

Let be $w = (x, y, z)$ any position vector, the skew-symmetric matrix $\mathbf{S}(w)$ associated with w is

$$\mathbf{S}(w) = \begin{bmatrix} 0 & -z & y \\ z & 0 & -x \\ -y & x & 0 \end{bmatrix}.$$

Under *Steiner's theorem* the inertial contributions of the i-th link can be obtained with respect to the total mass center $\mathbf{O_{ci}}$ as

$$\mathbf{I_i^i} = \sum_{j=1}^{p} \mathbf{I_{i,j}} + m_{i,j} \mathbf{S^T}(\mathbf{r_{i,j}}) \mathbf{S}(\mathbf{r_{i,j}}), \tag{71}$$

where $\mathbf{I_{i,j}}$ is the invariant inertia tensor for the j-th element with respect to the i-th frame. $\mathbf{r_{i,j}}$ is the position vector that represents the center mass location between the j-th element $\mathbf{O_{c_{i,j}}}$ and the total mass center $\mathbf{O_{ci}}$ of the i-th frame (Fig. 5), i.e.

$$\mathbf{r_{i,j}} = (\mathbf{O_{c_{i,j}}} - \mathbf{O_{ci}}). \tag{72}$$

IV. CONCURRENT OPTIMIZATION FOR SELECTION AND CONTROL OF AC SERVO MOTORS

This paper is focused on obtaining the best set of motors, that optimizes three performance objectives, energy consumption, tracking error and motors total weight, subject to limits and operating ranges of feasible motors and the closed-loop robot dynamics (Fig. 6).

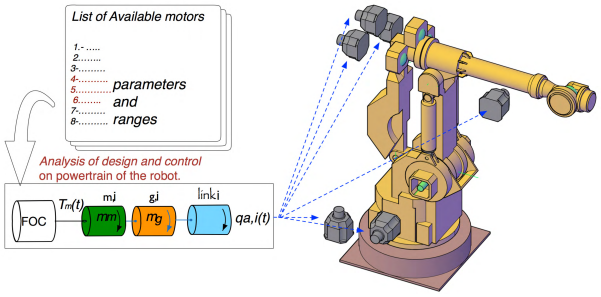

FIGURE 6. Available motors and indexes selection for the actuated joints.

Objective functions and decision variables are presented as follows.

A. OBJECTIVE FUNCTIONS

Three objective functions are considered to be optimized.

1) ENERGY CONSUMPTION

Based on [32] the power losses, on each k-th motor of the powertrain, are electrical $\mathbf{W_E}$ and mechanical $\mathbf{W_M}$, which are denoted as

$$W_{E,k} = R_{s,k}(i_{d,k}^2 + i_{q,k}^2), \quad k = 1, \ldots, n_a \tag{73}$$
$$W_{M,k} = T_{m,k} n_{r,k} q_{a,k}, \quad k = 1, \ldots, n_a. \tag{74}$$

The energy balance of all the motors can be described by

$$\mathbf{P_M} = \mathbf{W_E} + \mathbf{W_M}. \tag{75}$$

Then, the objective consists on minimizing energy consumption of motors

$$f_1 = \int_0^{t_f} \mathbf{P_M}(t)^T \mathbf{P_M}(t) dt, \tag{76}$$

by selecting the best motor parameters and tuning control gains, where t_f is the final cycle time of the task.

2) TRACKING ERROR

The tracking error objective is given by

$$f_2 = \int_0^{t_f} \mathbf{e}(t)^T \mathbf{e}(t) dt. \tag{77}$$

where $\mathbf{e}(t)$ is the position error given by (39).

3) TOTAL WEIGHT OF AC SERVOMOTORS

The objective is to minimize the total weight of actuators, by selecting low-weight motors that can properly drive the required task i.e.,

$$f_3 = \sum_{k=1}^{n_a} m_{m,k}, \tag{78}$$

where $m_{m,k}$ is the mass of the k-th motor added to the powertrain of the robot.

B. DECISION VARIABLES

1) INTEGER DECISION VECTOR

Let's consider that there is an integer index $z_{m,k}$ associated with each possible motor, so if in the catalog there are d_m candidate motors, then $1 \leq z_{m,k} \leq d_m, k = 1, \ldots, n_a$. Thus, a design decision vector $\mathbf{z_m} \in \mathbb{Z}^{n_a}$ with $\mathbf{z_m} = [z_{m,1}, z_{m,2}, \ldots, z_{m,n_a}]$ is to be found by the optimization algorithm.

2) CONTINUOUS DECISION VECTOR

Gains of the FOC controller at each actuated joint, conform a decision vector $\mathbf{x_c} = [[k_{p_1,q}, \ldots, k_{p_{n_a},q}], [k_{p_1,d}, \ldots, k_{p_{n_a},d}], [k_{I_1,q}, \ldots, k_{I_{n_a},q}], [k_{I_1,d}, \ldots, k_{I_{n_a},d}], [k_{1,1}, \ldots, k_{1,n_a}], [k_{2,1}, \ldots, k_{2,n_a}]]$, whose entries belong to the diagonal matrices $\mathbf{K}_{p,q}$, $\mathbf{K}_{p,d}$, $\mathbf{K}_{I,q}$, $\mathbf{K}_{I,d}$, $\mathbf{K_1}$ and $\mathbf{K_2}$ respectively. Moreover, control gains should be positive, so

$$x_{c,l} > 0, \quad l = 1, \ldots, 6n_a. \tag{79}$$

C. CONSTRAINTS

To avoid overexertion, heating or damage on the powertrain of the robot, the proposed constraints for the optimization problem are: the dynamic equation of the closed-loop control system given by (46)-(49), the mechanical and electrical characteristics of feasible motors (50)-(65), and changes in the inertial parameters (69), (70) and (71).

D. CONCURRENT OPTIMIZATION PROBLEM

In order to optimally select the robot actuators, a multi-objective dynamic optimization problem is stated as, finding a decision vector $\mathbf{X}^* = \left[\mathbf{z_m^*}, \mathbf{x_c^*}\right]^\mathbf{T}$, that optimizes the objective function vector

$$\min_{\mathbf{X}} \mathbf{F} = [f_1, f_2, f_3], \tag{80}$$

subject to:

- The closed-loop dynamics of the mechatronic model system (46)-(49).
- The motors feasibility criterion related to mechanical and electrical characteristics, and constraints of a coupled motor and reducer, given by (50)-(65).
- Changes in mass and inertial parameters and their effects on the dynamics of the manipulator (69), (70) and (71).

E. NSGA-II GENETIC ALGORITHM

The NSGA-II algorithm is able for good spread, diversity of solutions, and convergence near to the true Pareto optimal front. A flowchart of an iteration of NSGA-II is shown in Fig. (7).

The algorithm is as follows,

1) Create the initial population $P_t(N)$ with N individuals (or chromosomes) by using random design variables, where the first generation is $t = 1$, and the i_x-th chromosome has $7 \times n_a$ design variables composed by continuous and discrete design variables $\mathbf{X^{i_x}} = \left[\mathbf{z_m^{i_x}}, \mathbf{x_c^{i_x}}\right]^\mathbf{T}$, and $i_x = 1, \ldots, N$.

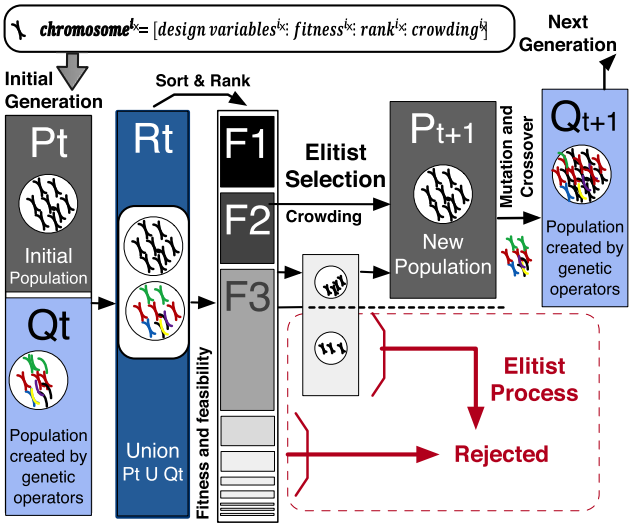

FIGURE 7. One generation of the NSGA-II algorithm.

2) Create a new population of M chromosomes $Q_t(M)$ from the population $P_t(N)$, by applying the genetic algorithm operators such as selection, crossover and mutation.
3) Evaluate each objective function, obtaining the *fitness* vector $[f_1^{i_x}, f_2^{i_x}, f_3^{i_x}]$, and verify for the chromosome i_x if it fulfills with the constraints feasibility
4) Merge population $P_t(N)$ with $Q_t(M)$ in order to create a new population $R_t(N+M)$, i.e. $R_t = P_t \bigcup Q_t$
5) Sort $R_t(N+M)$ and hierarchize them according to the dominance of the chromosomes to form r fronts, i.e. $F_t(1, \ldots, r)$ (*ranking*).
6) By using an elitist process, select the best population to form r from the r ranks created (non-dominated chromosomes), where $r^* \leq r$.
7) Apply the crowding distance process on the next fronts F_{r^*+1}, by adding the best chromosomes in order to have the next new population, i.e. until $size(P_{t+1}) = N$.
8) Since we have the new population P_{t+1}, where $t = t+1$ represents the next generation, repeat all the process from step (2) until the maximum number of generations is attained.

V. OPTIMAL ACTUATOR SELECTION RESULTS

A parallel industrial robot manipulator of six DOF of the brand Nachi Robotics Systems (Fig. 8) driven by PMSMs is considered as the case study. Fig. 9 shows the robot configuration, where $d_0 = 0.265$ [m], $a_0 = 0.25$ [m], $d_1 = 0.71$ [m], $a_2 = a_4 = 1.045$ [m], $a_3 = a_{52} = 0.41$ [m], $a_5 = 1.70$ [m], $d_y = 0.15$ [m], and $a_6 = 0.235$ [m].

Inertial parameters of the robot are shown in Table 1, where m_i is the mass of the i-th link and $\mathbf{O_{ci}} = [x_{ci}, y_{ci}, z_{ci}]^T$ is the mass center location of the i-th link with respect to the local frame.

FIGURE 8. Industrial robot manipulator of particular case.

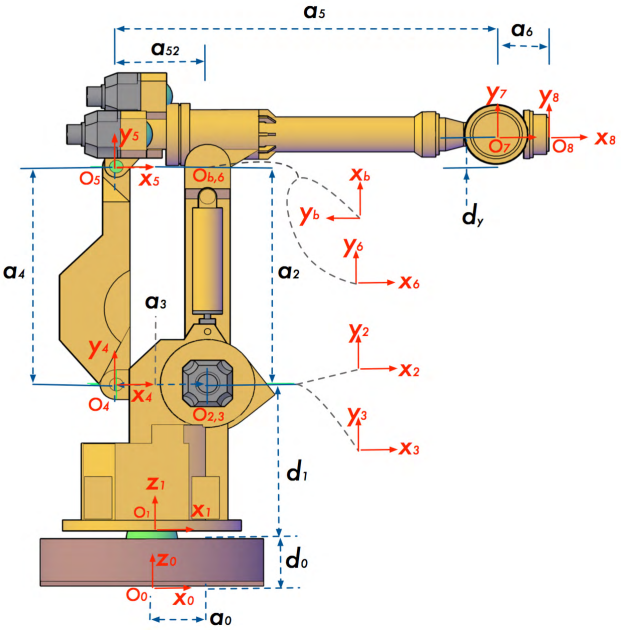

FIGURE 9. Configuration of the industrial robot manipulator.

Considering that $\mathbf{I_i^i}$ is the tensor of inertia of the i-th link with respect to the i-th frame, it is defined as

$$\mathbf{I_i^i} = \begin{bmatrix} I^i_{xx,i} & I^i_{xy,i} & I^i_{xz,i} \\ I^i_{yx,i} & I^i_{yy,i} & I^i_{yz,i} \\ I^i_{zx,i} & I^i_{zy,i} & I^i_{zz,i} \end{bmatrix}. \tag{81}$$

Then,

$$\mathbf{I_{base}^{I_{base}}} = \begin{bmatrix} 46.5451 & 0 & 0 \\ 0 & 46.5451 & 0 \\ 0 & 0 & 66.9080 \end{bmatrix}, \tag{82}$$

$$\mathbf{I_1^1} = \begin{bmatrix} 264.2562 & 0.0006 & -60.3371 \\ 0.0006 & 272.8590 & 0.0018 \\ -60.3371 & 0.0018 & 85.7910 \end{bmatrix}, \tag{83}$$

TABLE 1. Physical parameters of the robot.

Link	m $[Kg]$	$x_{c,i}$ $[(m]$	$y_{c,i}$ $[m]$	$z_{c,i}$ $[m]$
base	413.6813	0	0	0.1569
1	818.8935	0.106276	0	0.436926
2	316.6365	0.453425	0	0.001040
3	46.2946	0.199324	0	0
4	196.8490	0.483409	0.068096	-0.006479
5	498.6857	0.577954	0.163186	0.002786
6	72.0539	0.063614	0	0.039218

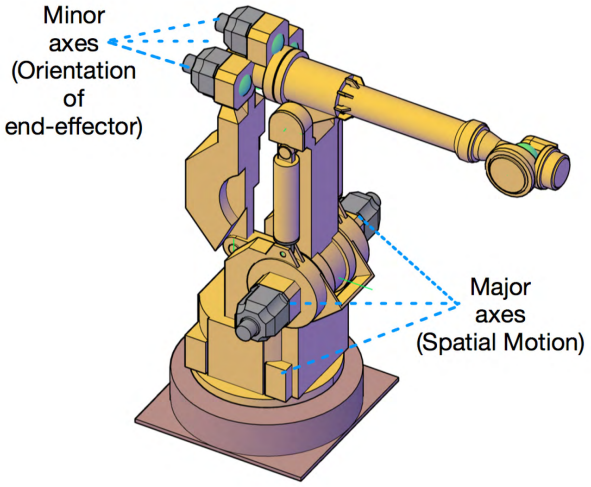

FIGURE 10. Major and minor robot axes.

$$\mathbf{I}_2^2 = \begin{bmatrix} 7.2241 & 0 & -0.1493 \\ 0 & 125.5378 & 0 \\ -0.1493 & 0 & 123.6983 \end{bmatrix}, \quad (84)$$

$$\mathbf{I}_3^3 = \begin{bmatrix} 0.1510 & 0 & 0 \\ 0 & 2.9732 & 0 \\ 0 & 0 & 2.9976 \end{bmatrix}, \quad (85)$$

$$\mathbf{I}_4^4 = \begin{bmatrix} 4.1378 & -4.8865 & 1.0589 \\ -4.8865 & 62.4879 & 0.0957 \\ 1.0589 & 0.0957 & 63.7890 \end{bmatrix}, \quad (86)$$

$$\mathbf{I}_5^5 = \begin{bmatrix} 23.0635 & -44.4309 & -0.3522 \\ -44.4309 & 323.2139 & -0.2103 \\ -0.3522 & -0.2103 & 334.9734 \end{bmatrix}, \quad (87)$$

and

$$\mathbf{I}_6^6 = \begin{bmatrix} 0.9341 & 0 & 0.0375 \\ 0 & 1.6148 & 0 \\ 0.0375 & 0 & 1.2826 \end{bmatrix}, \quad (88)$$

where all the entries of the inertia tensors are in $[Kg \cdot m^2]$.

The joints are actuated by PMSM Synchronous AC servo motors, each one coupled with a reducer.

Selection of motors for the major axes of the robot is carried out to test the proposed method. Then, the robot is considered as a 3 DOF spatial robot, Fig 10. In this way, the effects of control and motions of the orientation of the wrist do not affect the selection method.

The desired task consists of taking an aluminum plate adding load to the end effector, from an initial to a final point inside the workspace. The geometry of the load is length $=$ 0.3 $[m]$, height $=$ 0.3 $[m]$, and deep $=$ 0.1 $[m]$, with a total mass of 24.2856 $[Kg]$. The mass center location is $O_{c,load} = [0.0500, 0, 0]^T$, and the inertia tensor of the load is

$$\mathbf{I}_{\mathbf{load}}^{\mathbf{load}} = \begin{bmatrix} 0.3643 & 0 & 0 \\ 0 & 0.2024 & 0 \\ 0 & 0 & 0.2024 \end{bmatrix}. \quad (89)$$

The initial P_1 and final P_2 desired points (in $[m]$) of the task are, respectively

$$P_1 = [0, -1, 0.5]^T, \quad (90)$$

$$P_2 = [1.825, 0, 2.17]^T, \quad (91)$$

with a final time of $t_f = 8\ s$. The transmission ratio on the reducers of the three major axes are $n_{r,1} = 1:100$, $n_{r,2} = 1:120$, $n_{r,3} = 1:120$.

The settling time is $t_e = 7s$ to ensure that the robot achieves the final point, where the steady-state position profiles are within 2% of the required final value.

The objective of this particular case consists of redesigning the robot powertrain, by an appropriate selection of *off the shelf* AC servomotors for the three major axes of the robot, and assigning a proper set of control gains for the FOC control for minimum energy consumption, minimum tracking error and the minimum weight of selected motors.

Then, by using the genetic algorithm it is required to obtain a decision vector $\mathbf{X}^*$, composed by discrete and continuous design variables ($\mathbf{z}_\mathbf{m}^* \in \mathbb{Z}^3$ and $\mathbf{x}_\mathbf{c}^* \in \mathbb{R}^{18}$) as

$$\mathbf{X}^* = \left[\mathbf{z}_\mathbf{m}^*, \mathbf{x}_\mathbf{c}^*\right]^\mathbf{T}, \quad (92)$$

to minimize the objective function vector

$$\min_{\mathbf{X}} \mathbf{F} = [f_1, f_2, f_3], \quad (93)$$

subject to:

- The closed-loop dynamics of the mechatronic system.
- Changes of inertial parameters.
- The use of a proposed catalog list that relates each index selection of motor of the discrete vector (Appendix).
- The criteria for feasible AC servomotors related to mechanical and electrical constraints.
- The settling time $t_e = 7$ s, within an error of 2% with respect to the desired final value.
- A required cycle time of $t_f = 8$ s.

For the genetic algorithm, a population of 100 chromosomes is proposed, where at 1300 generations a set of non-dominated solutions is obtained, fulfilling with all the constraints. The parameter values for the NSGA-II algorithm can be seen in Table 2.

TABLE 2. NSGA-II algorithm parameters.

Symbol	Parameter	Value
N_{pop}	Size of population	100
gen_{max}	Maximum number of generations	1300
P_{cross}	Crossover Probability	0.7
C_{cross}	Crossover index	20
P_{mut}	Mutation Probability	1/21
C_{mut}	Mutation index	20

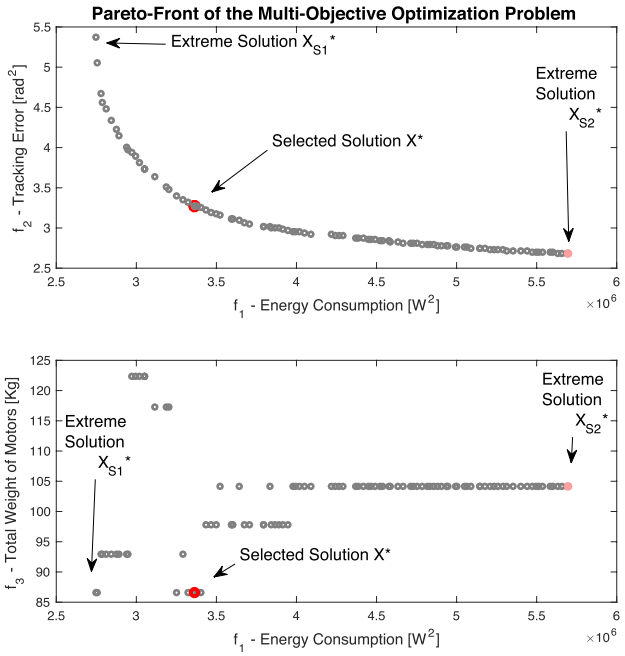

FIGURE 11. Pareto front for motor selection.

A. SIMULATION RESULTS

A set of non-dominated solutions is obtained by using the NSGA-II algorithm, resulting in the Pareto front in Fig. 11. It can be seen that for lower energy consumption a higher tracking error is obtained, this fact is explained by the rationale that more energy is required to reach the desired motion quickly. Regarding the total weight of actuators, there can be different combinations of motors to get feasible solutions; however, for lower tracking error the combination set of motors seems to stand around 105 $[Kg]$, this may infer that there are few combinations of energetically capable candidate motors to achieve this tracking error, and in order to achieve the minimal tracking error more energy consumption is required.

In a multi-objective optimization problem, the concept of the best solution turns subjective, since the fitness value of each objective function cannot be minimized without worsening the value of some other objective. Thus, the designer has to select, in a subjective manner, one non-dominated solution from the obtained Pareto-Front to best satisfy the desired objectives.

Some authors suggest a Post analysis of Pareto-front [33], searching the *Utopian point* from the non-dominated points

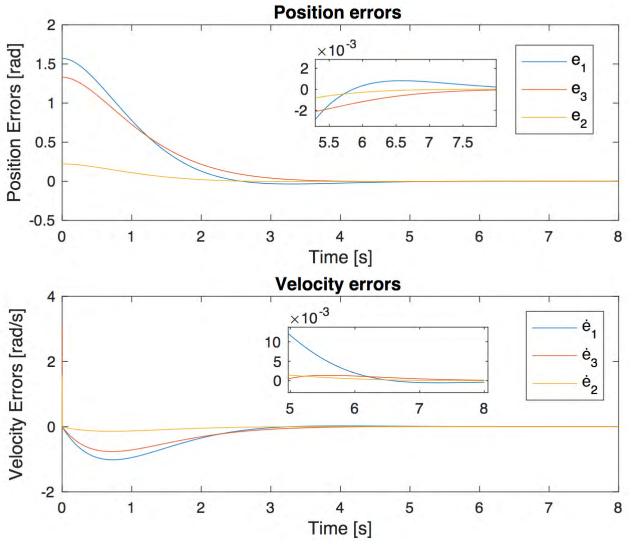

FIGURE 12. Position and velocity errors of actuated Joints.

of objective functions, or the most equality-weighted solution. However, they select a local solution from the Pareto-Optimal set. Therefore, we consider obtaining all the spread set of solutions to form the Pareto-Front.

Let us consider S_1 and S_2 as are the extreme solutions among possible solutions at the Pareto-front (Fig. 11), where S_1 is the solution with minimum energy consumption during the task and S_2 with minimum tracking error during the task from the obtained Front.

According to compared fitness results between S_1 and S_2, and the different trade-offs between the three objective functions shown in Table 3, a point X^* is subjectively selected as the solution of the proposed multi-objective problem.

TABLE 3. Comparative fitness.

Solution	f_1- Weight $[Kg]$	f_2- Tracking $[rad^2]$	f_3 - Energy $[W^2]$
S_1	86.53	5.376	2.746×10^6
S_2	104.1	2.684	5.698×10^5
X^*	86.53	3.27	3.36×10^6

1) SELECTED SOLUTION FOR THE MULTI-OBJECTIVE OPTIMIZATION PROBLEM

In order to show the performance of the complete closed-loop system for a particular solution, we select the chromosome denoted as X^*(chromosome No. 63) which satisfies all considered constraints and seems one equality-weighted solution between energy consumption and tracking error, and with minimal weight as possible. The decision vector values for the selected solution are the following,

- Indexes of selection for motors $\mathbf{z} = [\mathbf{z_{m,1}}, \mathbf{z_{m,2}}, \mathbf{z_{m,3}}]$: $\mathbf{z}(X^*) = [17, 28, 26]$.
- Control gain values for the FOC controllers $\mathbf{x_c} = [diag\{\mathbf{K_{P,q}}\}; diag\{\mathbf{K_{P,d}}\}; diag\{\mathbf{K_{I,q}}\}; diag\{\mathbf{K_{I,d}}\}; diag\{\mathbf{K_1}\}; diag\{\mathbf{K_2}\}]$:

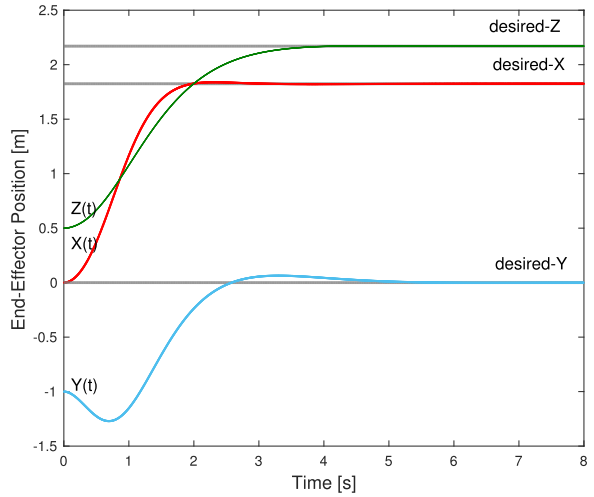

FIGURE 13. Tracking of desired positions In Cartesian space.

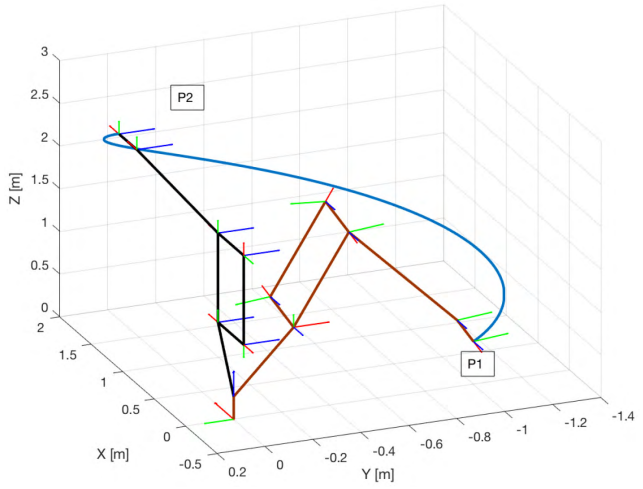

FIGURE 14. End-effector resulting trajectory in Cartesian space. At each joint $\mathbf{Oc}_i = (x_i, y_i, z_i) = (red, green, blue)$.

$$\mathbf{x_c}(X^*) = \{[0.0008, 0.0053, 0.107]; [3.88, 3.24, 2.13]; [9.4203, 9.5654, 8.1114]; [4.5610, 2.8316, 7.6887]; [760.09, 810.376, 809.77]; [785.81, 998.33, 850.88]\}.$$

Position and velocity errors of actuated joints (three major axes) are shown in Fig. 12, it can be seen that positions are near to the desired point since $t \geq 5$ $[s]$; however, the controller has to ensure the final point constraint one second before the final time t_f. The time behaviour of the end effector position from P_1 to P_2 is shown in Fig. 13, where variations within the 2% final value condition are accomplished at $t_e = 7$ $[s]$.

The obtained trajectory in Cartesian space is shown in Fig. 14, which is the resulting trajectory of the end-effector where the robot handles the load from P_1 to P_2. In the figure, each local frame axes is shown at each joint.

According to the FOC technique, all desired currents $\mathbf{I_d^*}$ in the d axis are zero. However, these currents are used to calculated errors for the PI inner controllers in order to

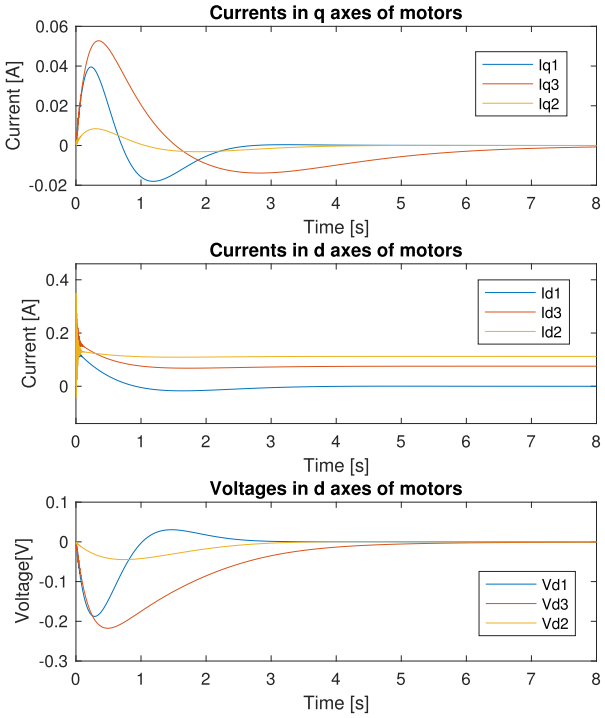

FIGURE 15. Currents of actuated joints in q-d axes and voltages convergence on d axes.

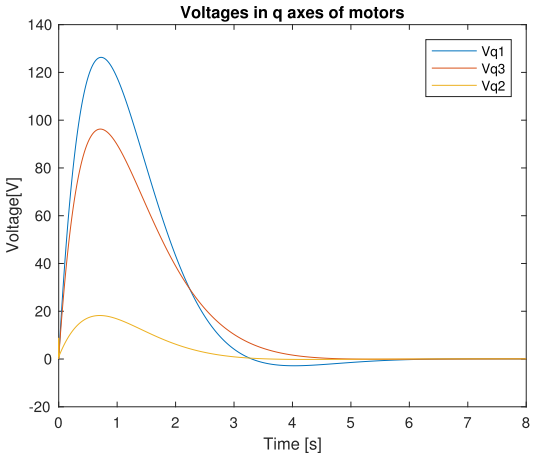

FIGURE 16. Voltages in q axes.

achieve the desired voltages in the d axis $\mathbf{V_d^*}$. Then, currents tend to a constant value to yield convergence of the voltages of the d axes to zero. Thus, the currents in the q axis are in quadrature, which totally defines the current-torque control on the powertrain. The response transition of currents in the q and d axes, and transition of voltages in the d axis, before converging to zero are shown in Figure 15.

The control voltages in the q axis were obtained by using the desired currents and voltages in the d axis, as a result of the PI loop controllers. The q axis voltages profiles are shown in Fig. 16.

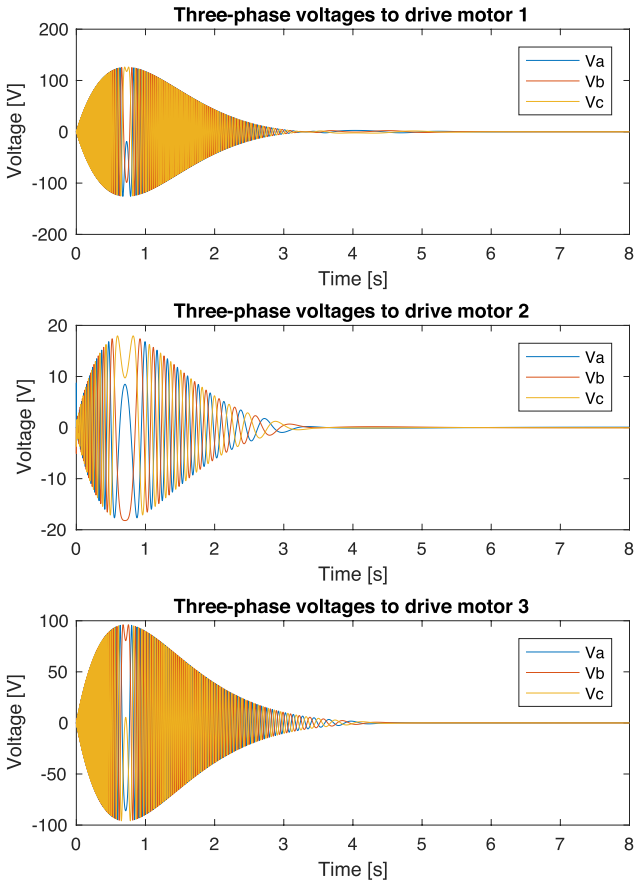

FIGURE 17. Three-phase voltages to drive selected motors.

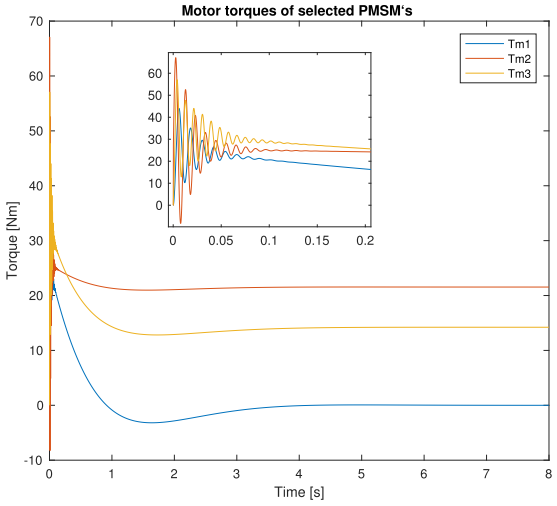

FIGURE 18. Motor torques of actuated joints.

By using the Clarke and Park Transform Matrix, we obtain the real three phase voltages required by the FOC control of the selected motors. These voltage profiles are sent to the inverter to drive the motors, which are shown in Fig. 17.

Finally, motor and load torques on actuated joints are shown in Figures 18 and 19 respectively, where at motion beginning, it can be seen high peak torques. Note that torques of Fig. 19 are the load profiles that have to be driven by the powertrain. Because of the transmission design, inside the robot, the transmission reduction ratio, and the reducer given by the own structure design of the robot, the motor torques are lower than load torques, since they depend on the interaction of motor-reducer to drive the required loads. In this case, with the selected motors, the motor torques to drive the given load torques, can be shown in Fig 18.

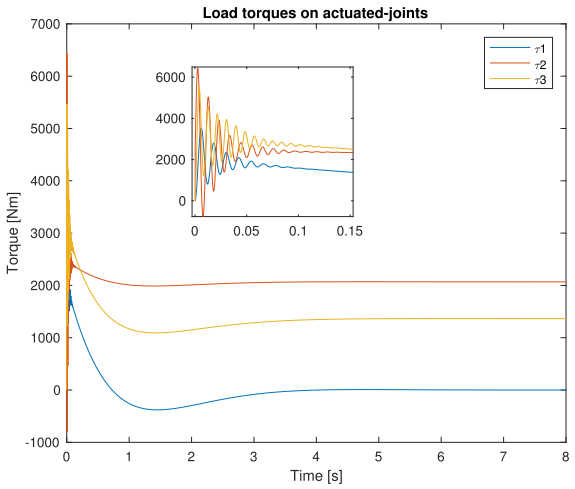

FIGURE 19. Load torques of actuated joints.

TABLE 4. Catalog list of motors. Mechanical limits of operation.

Motor index	Brand	Model	$T_{M,N}$ $[Nm]$	$T_{M,max}$ $[Nm]$	$\omega_{M,N}$ $[rpm]$	$\omega_{M,max}$ $[rpm]$
1	HNC Electric	130-060M25	6	18	2500	7500
2	HNC Electric	S130-2-077M20	7.7	23.1	2500	7500
3	HNC Electric	S130-2-077M25	7.7	23.1	2000	6000
4	HNC Electric	S130-2-077M30	7.7	23.1	3000	9000
5	HNC Electric	S130-100M25	10	30	2500	7500
6	HNC Electric	S130-150M15	15	45	1500	4500
7	HNC Electric	S130-150M25	15	45	2500	7500
8	HNC Electric	S150-150M25	15	45	2500	7500
9	HNC Electric	S150-180M20	18	54	2000	6000
10	HNC Electric	S150-230M20	23	69	2000	6000
11	HNC Electric	S150-270M20	27	81	2000	6000
12	HNC Electric	S180-2-270M15	27	67	1500	4500
13	HNC Electric	S180-2-350M10	35	70	1000	3000
14	HNC Electric	S180-2-350M15	35	70	1500	4500
15	HNC Electric	S180-2-480M15	48	96	1500	4500
16	ABB. Baldor	BSM100N-1150	14	56	2000	4000
17	ABB. Baldor	BSM100N-1250	14	56	1200	4000
18	ABB. Baldor	BSM100N-2150	23	92	2000	4000
19	ABB. Baldor	BSM100N-2250	23	92	1200	4000
20	ABB. Baldor	BSM100N-3150	34	136	2000	4000
21	ABB. Baldor	BSM100N-3250	34	136	1200	4000
22	ABB. Baldor	BSM100N-4150	40	160	2000	4000
23	ABB. Baldor	BSM100N-4250	40	160	1200	4000
24	ABB. Baldor	BSM90C-4150	10	30	2400	7000
25	ABB. Baldor	BSM100C-4150	20	60	2400	7000
26	ABB. Baldor	BSM100C-4250	20	60	1200	7000
27	ABB. Baldor	BSM100C-5150	25	75	2400	7000
28	ABB. Baldor	BSM100C-5250	25	75	1200	7000
29	ABB. Baldor	BSM100C-6150	30	90	2000	7000
30	ABB. Baldor	BSM100C-6250	30	90	1200	7000

TABLE 5. Catalog list of motors. Electrical limits of operation.

Motor index	P_N $[10^3 W]$	V_{bus} $[V]$	I_N $[A]$	I_{max} $[A]$
1	1.5	220	6	18
2	1.6	220	6	18
3	2	220	7.5	22.5
4	2.4	220	9	27
5	2.6	220	10	30
6	2.3	220	9.5	28.5
7	3.8	220	17	51
8	3.8	220	16.5	49.5
9	3.6	220	16.5	49.5
10	4.7	220	20.50	61.50
11	5.5	220	20.50	61.50
12	4.3	220	16	48
13	3.7	220	16	48
14	5.5	220	24	72
15	7.5	220	32	96
16	3	320	9.40	34
17	1.8	320	5.90	21.20
18	5	320	15.50	55.80
19	3.15	320	9.90	35.80
20	6.7	320	21	75.80
21	4.7	320	14.70	53.10
22	8.6	320	26.90	97.10
23	5.3	320	16.80	60.70
24	2.5	320	8.020	20.40
25	5.4	320	16.80	42.90
26	3.4	320	10.60	26.90
27	6.7	320	21	53.600
28	4.2	320	13	33.100
29	8	320	24	61.300
30	4.5	320	14.10	36

TABLE 6. Catalog list of motors. Mechanical parameters.

Motor index	J_m $[Kg \cdot m^2]$	$size_{(length,base,height)}$ $[m, m, m]$	d_m $[m]$	m_m $[Kg]$
1	1.54e-07	[0.22 , 0.13 , 0.13]	0.022	11.40
2	1.54e-07	[0.22, 0.13, 0.13]	0.022	11.40
3	2.01e-07	[0.23, 0.13, 0.13]	0.022	11.70
4	2.01e-07	[0.23, 0.13, 0.13]	0.022	11.70
5	2.59e-07	[0.25, 0.13, 0.13]	0.022	13.30
6	3.24e-07	[0.30, 0.13, 0.13]	0.022	16.90
7	3.24e-07	[0.30, 0.13, 0.13]	0.022	16.90
8	6.15e-07	[0.29, 0.152, 0.15]	0.028	24.40
9	6.33e-07	[0.31, 0.152, 0.15]	0.028	26.20
10	8.94e-07	[0.34, 0.152, 0.15]	0.028	29.20
11	1.12e-06	[0.36, 0.152, 0.15]	0.028	32.20
12	6.10e-07	[0.32, 0.18, 0.18]	0.035	30.50
13	8.60e-07	[0.35, 0.18, 0.18]	0.035	35.50
14	8.60e-07	[0.35, 0.18, 0.18]	0.035	35.50
15	9.50e-07	[0.40, 0.18, 0.18]	0.035	45
16	1.35e-03	0.27, 0.14, 0.14]	0.028	19.978
17	1.35e-03	[0.146, 0.14 , 0.14]	0.028	19.978
18	2.21e-03	[0.32, 0.14, 0.14]	0.028	26.278
19	2.21e-03	[0.32, 0.14, 0.14]	0.028	26.278
20	3.08e-03	[0.36, 0.14, 0.14]	0.028	32.578
21	3.08e-03	[0.37, 0.14, 0.14]	0.028	32.578
22	3.94e-03	[0.42, 0.14, 0.14]	0.028	38.978
23	3.94e-03	[0.42, 0.14, 0.14]	0.028	38.978
24	3.38e-03	0.41, 0.12, 0.12]	0.028	20.30362
25	6.75e-03	0.34, 0.14, 0.14]	0.028	30.778
26	6.75e-03	0.34, 0.14, 0.14]	0.028	30.778
27	8.44e-03	0.38, 0.14, 0.14]	0.028	35.778
28	8.44e-03	0.38, 0.14, 0.14]	0.028	35.778
29	10.1e-03	0.42, 0.14, 0.14]	0.028	40.778
30	10.1e-03	0.42, 0.14, 0.14]	0.028	40.778

This fact represents an advantage of selecting AC Servo Motors (over DC motors), as it is possible to drive high peak torques and high accuracy of the required motion, with low energy consumption. Then, regardless high or low torque profiles, the selected motors satisfy all the constraints and can operate the required load according to their own continuous and dynamics operation zones, whose limit values were given by their own manufacturer designers to avoid overheating, damage or overexertion.

VI. CONCLUSIONS

A concurrent optimization method to optimally select AC servomotors for industrial manipulators is presented in this paper, obtaining feasible solutions for a required task. For this, energy consumption, tracking error and the total weight of motors are proposed to be minimized according to their own operating zones and thermal, mechanical and electrical constraints to avoid overheating and overexertion of the powertrain before to make a final decision of selection.

According to the obtained results, for more diversity of feasible solutions higher quantity of candidate motors is needed in the proposed motor list. However, due to the trade-offs between the proposed objectives, regardless the number of candidate motors, for lower tracking error higher energy consumption is needed on the candidate motors, and for more energy consumption a lower set of motor combinations with minimum total weight as possible.

Moreover, it has been observed that motor capabilities are generally proportional to their weight, candidate motors with wide dynamic and continuous range to follow high dynamic loads are commonly weightier. Since more than one motor can be added along the robot's kinematic chain, the actuators' weight directly affect the closed-loop dynamic response. Thus, masses and inertial parameters involved at each link of the robot should be considered in a motor selection process for robots.

The proposed methodology concurrently involves design and control parameters to study a complete insight into the physics of the system, such as total weight, energy, physical limitations, control effects, loads, and so on, thus yielding

TABLE 7. Catalog list of motors. Electrical parameters.

Motor index	$L_{q,d}$ $[mH]$	λ_{af} $[Wb \cdot s]$	R_s $[\Omega]$	$Poles$ $[-]$	K_e $[V_{pk-pk}/Krpm]$
1	1.12	0.051	0.302	8	37.34
2	1.14	0.051	0.33	8	37.34
3	0.96	0.055	0.227	8	40.03
4	0.616	0. 044	0.141	8	32.22
5	0.629	0. 053	0.131	8	38.76
6	1.185	0. 093	0.229	8	68.13
7	0.299	0. 046	0.051	8	34.07
8	0.358	0.048	0.058	8	35.09
9	0.42	0.057	0.066	8	41.07
10	0.337	0. 059	0.048	8	43.46
11	0.383	0. 069	0.0545	8	50.5
12	0.87	0.141	0.14	8	103
13	1.64	0.284	0.155	8	134
14	0.5	0.124	0.07	8	90
15	0.385	0.129	0.052	8	94
16	4.4	0.193	0.60	8	140.4
17	12	0.31	1.5	8	225.3
18	2.2	0.194	0.266	8	140.8
19	5.5	0.301	0.58	8	219
20	1.8	0.211	0.166	8	153.1
21	3.9	0.301	0.406	8	218.8
22	1.245	0.193	0.12	8	140.7
23	3.24	0.310	0.306	8	225.1
24	5.5	0.172	1.06	8	125
25	2.9	0.163	0.38	8	118.9
26	7.5	0.261	1	8	189.9
27	2.3	0.163	0.27	8	118.9
28	6.1	0.266	0.713	8	193.4
29	1.7	0. 172	0.246	8	125
30	5	0. 294	0.8	8	213.9

accurate descriptions of the system dynamics to be considered in optimal actuator selection processes.

Unlike traditional selection methods where control-models are not considered, the proposed method accurate more knowledge of the drive system dynamics, which represents a more reliable method to analyze the dynamic response caused just by exchanging or installing different actuators on the powertrain in a given task.

Finally, the concurrent design approach is a methodology dealing with interdisciplinary design, obtaining feasible solutions for the analyzed system, where the interaction of subsystems is involved in accomplishing the desired objectives that are conflicting each other.

APPENDIX
LIST OF PMSM MOTORS

The following list of motors shows the ranges and parameters obtained from a commercial catalog of AC Servo Motor, whose values are given by the manufacturer.

REFERENCES

[1] S. Kurtenbach, T. Detert, M. Riedel, M. Hüsing, and B. Corves, "Motor positioning and drive train design for a 3-DOF robotic structure," in *New Trends in Mechanism and Machine Science*. Dordrecht, The Netherlands: Springer, 2013, pp. 217–225.

[2] J. A. Reyer and P. Y. Papalambros, "Combined optimal design and control with application to an electric DC motor," *J. Mech. Des.*, vol. 124, no. 2, pp. 183–191, 2002.

[3] A. Mohebbi, L. Baron, S. Achiche, and L. Birglen, "Trends in concurrent, multi-criteria and optimal design of mechatronic systems: A review," in *Proc. Int. Conf. Innov. Des. Manuf. (ICIDM)*, Aug. 2014, pp. 88–93.

[4] Z. Affi, B. El-Kribi, and L. Romdhane, "Advanced mechatronic design using a multi-objective genetic algorithm optimization of a motor-driven four-bar system," *Mechatronics*, vol. 17, no. 9, pp. 489–500, 2007.

[5] P. Chandhar and S. S. Das, "Multi-objective framework for dynamic optimization of OFDMA cellular systems," *IEEE Access*, vol. 4, pp. 1889–1914, 2016.

[6] M. Pettersson and J. Ölvander, "Drive train optimization for industrial robots," *IEEE Trans. Robot.*, vol. 25, no. 6, pp. 1419–1424, Dec. 2009.

[7] T. Brogårdh, "Robot control overview: An industrial perspective," *Model., Identificat. Control*, vol. 30, no. 3, p. 167, 2009.

[8] K. A. Pasch and W. P. Seering, "On the drive systems for high-performance machines," *J. Mech., Transmiss., Automat. Des.*, vol. 106, no. 1, pp. 102–108, 1984.

[9] F. Roos, H. Johansson, and J. Wikander, "Optimal selection of motor and gearhead in mechatronic applications," *Mechatronics*, vol. 16, no. 1, pp. 63–72, 2006.

[10] P. Chedmail and M. Gautier, "Optimum choice of robot actuators," *J. Eng. Ind.*, vol. 112, no. 4, pp. 361–367, 1990.

[11] H. J. van de Straete, P. Degezelle, J. De Schutter, and R. J. M. Belmans, "Servo motor selection criterion for mechatronic applications," *IEEE/ASME Trans. Mechatronics*, vol. 3, no. 1, pp. 43–50, Mar. 1998.

[12] A. Nicolescu, C. Avram, and M. Ivan, "Optimal servomotor selection algorithm for industrial robots and machine tools NC axis," *Proc. Manuf. Syst.*, vol. 9, no. 2, pp. 105–114, 2014.

[13] L. Zhou, S. Bai, and M. R. Hansen, "Design optimization on the drive train of a light-weight robotic arm," *Mechatronics*, vol. 21, no. 3, pp. 560–569, 2011.

[14] H. J. Van de Straete, J. De Schutter, and R. Belmans, "An efficient procedure for checking performance limits in servo drive selection and optimization," *IEEE/ASME Trans. Mechatronics*, vol. 4, no. 4, pp. 378–386, Dec. 1999.

[15] L. Ge, J. Chen, R. Li, and P. Liang, "Optimization design of drive system for industrial robots based on dynamic performance," *Ind. Robot, Int. J.*, vol. 44, no. 6, pp. 765–775, 2017.

[16] R. Krishnan, "Selection criteria for servo motor drives," *IEEE Trans. Ind. Appl.*, vol. TIA-23 no. 2, pp. 270–275, Mar. 1987.

[17] R.-J. Wai and K.-M. Lin, "Robust decoupled control of direct field-oriented induction motor drive," *IEEE Trans. Ind. Electron.*, vol. 52, no. 3, pp. 837–854, Jun. 2005.

[18] M. M. Fateh and M. Sadeghijaleh, "Voltage control strategy for direct-drive robots driven by permanent magnet synchronous motors," *Int. J. Eng. Trans. B, Appl.*, vol. 28, no. 5, pp. 709–716, 2014.

[19] M. C. Good, L. M. Sweet, and K. L. Strobel, "Dynamic models for control system design of integrated robot and drive systems," *J. Dyn. Syst., Meas., Control*, vol. 107, no. 1, pp. 53–59, 1985.

[20] N. Antonie, I. Borcoşi, A. Dincă, and M. Ionescu, "FOC control system of AC machines," in *Proc. 13th Eng. Fac. Sci. Conf.*, Anal. Univ. Constantin Brancusi, Târgu Jiu, Romania, 2008, pp. 307–312.

[21] G. S. Buja and M. P. Kazmierkowski, "Direct torque control of PWM inverter-fed AC motors—A survey," *IEEE Trans. Ind. Electron.*, vol. 51, no. 4, pp. 744–757, Aug. 2004.

[22] G. Cusimano, "A procedure for a suitable selection of laws of motion and electric drive systems under inertial loads," *Mech. Mach. Theory*, vol. 38, no. 6, pp. 519–533, 2003.

[23] C. Giancarlo, "Optimization of the choice of the system electric drive-device—Transmission for mechatronic applications," *Mech. Mach. Theory*, vol. 42, no. 1, pp. 48–65, 2007.

[24] C. Choi *et al.*, "A motor selection technique for designing a manipulator," in *Proc. Int. Conf. Control, Automat. Syst., (ICCAS)*, Oct. 2007, pp. 2487–2492.

[25] H. Giberti, S. Cinquemani, and G. Legnani, "Effects of transmission mechanical characteristics on the choice of a motor-reducer," *Mechatronics*, vol. 20, no. 5, pp. 604–610, 2010.

[26] K. Deb, A. Pratap, S. Agarwal, and T. Meyarivan, "A fast and elitist multiobjective genetic algorithm: NSGA-II," *IEEE Trans. Evol. Comput.*, vol. 6, no. 2, pp. 182–197, Apr. 2002.
[27] P. Zhai, P. Wang, R. Li, M. Wang, and S. Zhai, "Multi-objective optimization of six-bar mechanisms using NSGA-II," in *Proc. IEEE Int. Conf. Comput. Sci. Automat. Eng. (CSAE)*, vol. 2, May 2012, pp. 494–497.
[28] R. Tanabe, H. Ishibuchi, and A. Oyama, "Benchmarking multi-and many-objective evolutionary algorithms under two optimization scenarios," *IEEE Access*, vol. 5, pp. 19597–19619, 2017.
[29] B. Siciliano, L. Sciavicco, L. Villani, and G. Oriolo, *Robotics: Modelling, Planning and Control*. London, U.K.: Springer-Verlag, 2010, doi: 10.1007/978-1-84628-642-1.
[30] F. C. Park, J. Choi, and S. R. Ploen, "Symbolic formulation of closed chain dynamics in independent coordinates," *Mech. Mach. Theory*, vol. 34, no. 5, pp. 731–751, 1999.
[31] G. M. Freitas, A. C. Leite, and F. Lizarralde, "Kinematic control of constrained robotic systems," *SBA, Controle Automação Sociedade Brasileira Automatica*, vol. 22, no. 6, pp. 559–572, 2011.
[32] S. Morimoto, Y. Tong, Y. Takeda, and T. Hirasa, "Loss minimization control of permanent magnet synchronous motor drives," *IEEE Trans. Ind. Electron.*, vol. 41, no. 5, pp. 511–517, Oct. 1994.
[33] S. Parisi, A. Blank, T. Viernickel, and J. Peters, "Local-utopia policy selection for multi-objective reinforcement learning," in *Proc. IEEE Symp. Ser. Comput. Intell. (SSCI)*, Dec. 2016, pp. 1–7.

ERICK A. PADILLA-GARCIA received the B.S. degree in industrial robotics engineering from the National Polytechnic Institute (IPN) and the M.S. degree in electrical engineering, specialized in automatic control, from the Centro de Investigacióy de Estudios Avanzados (CINVESTAV-IPN), Guadalajara, Mexico, in 2011, where he is currently pursuing the Ph.D. degree in electrical engineering, specialized in mechatronics. His research interests include robotics, industrial manipulators, mechatronics, and design optimization.

ALEJANDRO RODRIGUEZ-ANGELES received the B.Sc. degree in communications and electronics from the National Polytechnic Institute (IPN), Mexico, in 1995, the M.Sc. degree in electrical engineering from the Centro de Investigacióy de Estudios Avanzados (CINVESTAV-IPN), Mexico, in 1997, and the Ph.D. degree in mechanical engineering from the Eindhoven University of Technology, Eindhoven, The Netherlands, in 2002. From 1998 to 2000, he was a Research Assistant with the Department of Applied Mathematics, University of Twente, Enschede, The Netherlands. From 2000 to 2002, he was a Research Assistant with the Eindhoven University of Technology. From 2003 to 2005, he was with the Mexican Institute of Petroleum, Mexico. Since 2005, he has been a Researcher with the Mechatronics Group, CINVESTAV-IPN. His research interests include synchronization, nonlinear control, model-based control, optimization, robotic systems, and supply chain systems.

JUVENAL R. RESÉNDIZ (SM'13) received the master's degree in automation, and the Ph.D. degree from Queretaro State University, Mexico, in 2010. He has been a Professor with the Autonomous University of Queretaro since 2008. He was a Visiting Professor with West Virginia University in 2012. He is currently the Chair of the Engineering Automation Program. He is also the Director of Technologic Link of all Queretaro State University. He has involved in industrial and academic automation projects for 15 years. He received several awards for his contributions in developing education technology. He belongs to the Mexican Academy of Sciences, the National Research Academy in Mexico, and seven associations regarding engineering issues. He is the IEEE Querétaro Section Past President.

CARLOS A. CRUZ-VILLAR received the B.S. degree in electronics engineering from the National Polytechnic Institute (IPN), Mexico, in 1996, and the Ph.D. degree in electrical engineering from the Centro de Investigacióy de Estudios Avanzados (CINVESTAV-IPN), Mexico, in 2001. Since 2001, he has been a Professor with the Electrical Engineering Department, Mechatronics Section, CINVESTAV-IPN. His research interests include the optimum design of mechatronic system and robust design.